Electronic Supplementary Material (ESI) for ChemComm.

Supporting information

Signatures of Technetium Oxidation States: A New Approach

Stephen Bauters[a,b], Andreas C. Scheinost[a,b], Katja Schmeide[b], Stephan Weiss[b], Kathy Dardenne[c], Jörg Rothe[c], Natalia Mayordomo[b], Robin Steudtner[b], Thorsten Stumpf[b], Ulrich Abram[d], Sergei M. Butorin[e,] and Kristina O. Kvashnina[a,b,*]*

[a] The Rossendorf Beamline at ESRF − The European Synchrotron, CS40220, 38043 Grenoble Cedex 9, France

[b] Helmholtz-Zentrum Dresden-Rossendorf (HZDR), Institute of Resource Ecology, Bautzner Landstr. 400, 01328 Dresden, Germany

[c] Karlsruhe Institute of Technology (KIT), Institute for Nuclear Waste Disposal (INE), P.O. Box 3640, D-76021 Karlsruhe, Germany

[d] Freie Universität Berlin, Institute of Chemistry and Biochemistry, Fabeckstr. 34/36, D-14195 Berlin, Germany

[e] Molecular and Condensed Matter Physics, Department of Physics and Astronomy, Uppsala University, P.O. Box 516, Uppsala, Sweden

Self-absorption effect in XAS

XAS in fluorescence mode determines X-ray photon absorption of the target element by detecting X-ray fluorescence, a correlated process. However, the produced X-ray fluorescence has to travel back through the sample to reach the detector. The attenuation that occurs on this travel path can significantly reduce the observed XAS oscillations, especially for more concentrated samples, creating a dampening effect.[1,2] Mathematical corrections can be employed to calculate the unaltered XAS signal, but are often not straightforward to apply and determine. A practical solution to prevent self-absorption effects is to measure with the sample under grazing exit conditions, causing the detected X-ray fluorescence to originate from only the topmost layer of sample. This recreates experimental conditions similar to the much more favourable thin sample case, reducing self-absorption effects significantly, as seen in Figure S1.

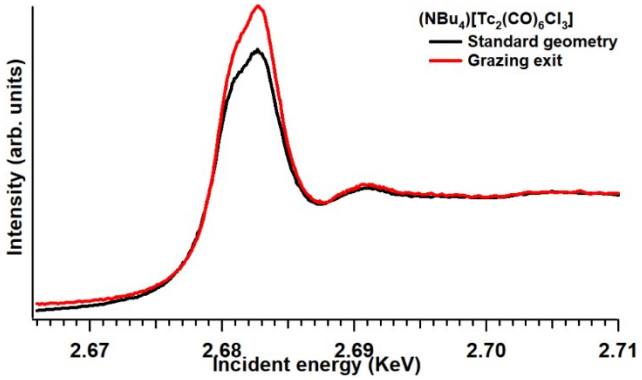

Figure S1 Tc L_3 XANES comparison in the 90-degree fluorescence detection geometry between the sample at a conventional angle (45 degrees to incoming beam and 45 degrees towards detector) and the sample in grazing exit configuration (~ 90 degrees to the incoming beam and ~ 0 towards the detector). A reduction in self-absorption effect can be seen in the grazing exit configuration.

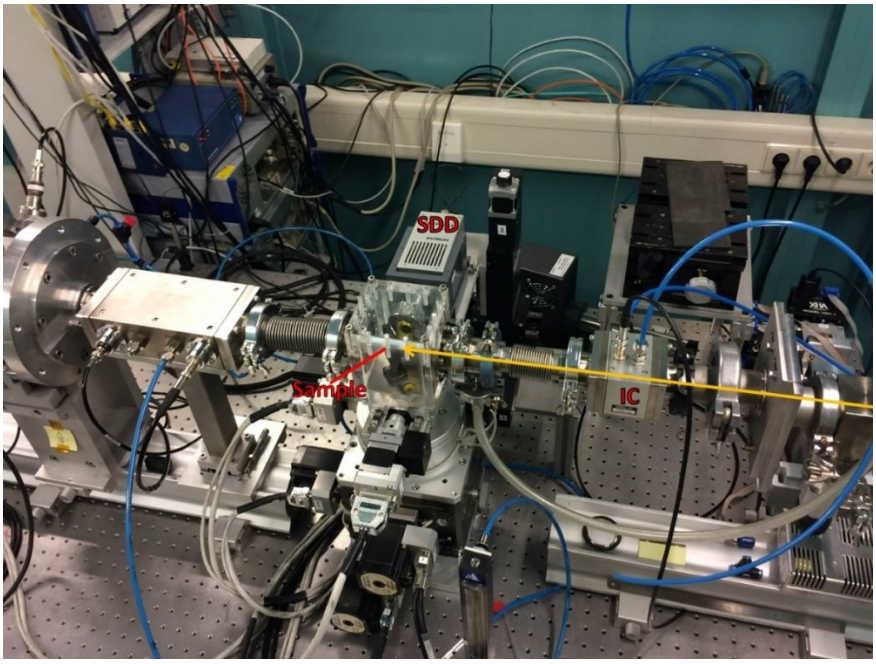

Figure S2. Experimental setup at the INE-Beamline of the KARA facility in Karlsruhe, Germany, showing the incoming beam passing through the ion chamber (IC) hitting the sample, with the SDD detector at a 90-degree angle. The entire setup from ion chamber until right before the SDD window is one connected He environment.

RAMAN

The spectra of the various Tc compounds (some samples are shown in Figure S3) were recorded using a Raman microscope (model Aramis, Horiba) with a 10-fold objective and a He/Ne (632 nm) laser with no filter, a pin-hole of 500 µm and a slit-width of 500 µm. Each spectrum was calculated as the average of three individual scans of 10 s. The samples were measured in different spots to ensure the homogeneity of the compounds. The Tc solids were measured using an in-house built Raman sample holder (Figure S3). The sample holder consists of a polyoxymethylene base with a 1 cm deep hole and a polyvinyl chloride lid. Both parts contain a 0.5 mm thick CaF_2 window that ensures the acquisition of spectra with high spectral purity due to its low interference. The solid samples were deposited on the CaF_2 placed in the base and the cell was closed with the lid.

Figure S3. (Top) Some samples of the Tc compounds and (bottom) assembled sample holders used for Raman measurements.

The spectra of the Tc-phosphine derivatives show three common peaks at 1007, 1592 and 3064 cm^{-1}, regardless on the Tc oxidation state (Figure S4). The peaks are related to the C-H alkene vibrations of the triphenylphosphine.[3] Additionally, a peak at 2984 cm^{-1} can be found in the spectrum of $[Tc^{III}Cl_3(PMe_2Ph)_3]$. This peak is caused by the C-H stretching vibrations in the CH_3 taking part of dimethylphenylphosphine.

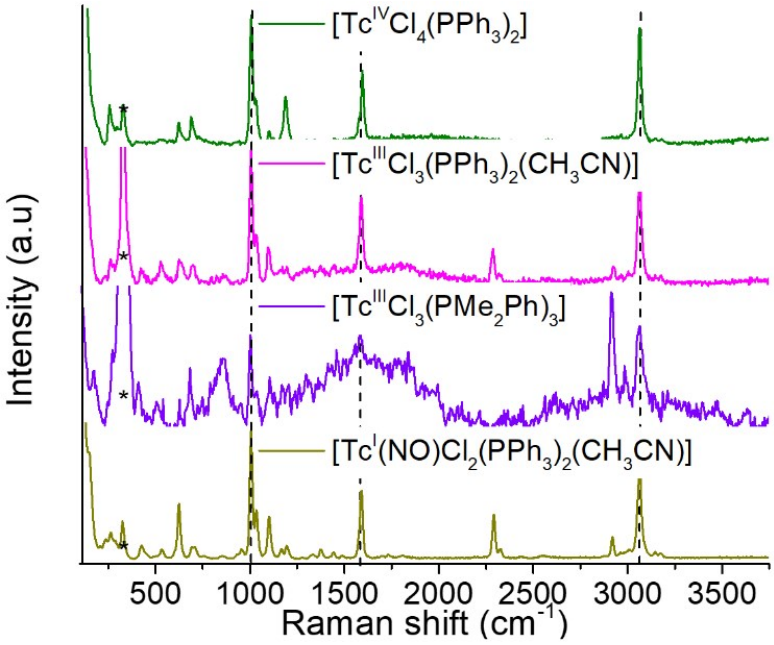

Figure S4. Raman spectra of various Tc complexes with phosphine-like ligands. Black dashed lines correspond to the main vibrations of phosphine ligands. The peak marked as (*) corresponds to CaF_2.

Moreover, two peaks are observed at 2291 and 2919 cm^{-1} in the spectrum of $Tc^{III}Cl_3(PPh_3)_2(CH_3CN)$] and [$Tc^{I}NO)Cl_2(PPh_3)_2(CH_3CN)$]. These peaks correspond to the C≡N stretching and C-H stretching in CH_3CN.[4]

The spectra of $(NH_4)_2[Tc^{IV}Br_6]$ and $(NH_4)_2[Tc^{IV}Cl_6]$ show two common bands at 1407 and 3144cm^{-1} (Figure S5), whose values are similar to the ones of crystalline NH_4^+ (3143 and 1400 cm^{-1}).[5] Likewise, the compounds that have NBu_4^+ as counter cation, show three common bands at 2876, 2933 and 2976 and 1457 cm^{-1}, except for $(NBu_4)[Tc^{VI}NBr_4]$, whose bands are slightly shifted to 2846, 2882, 2933 and 1443 cm^{-1}. These bands correspond to the CH_2 and CH_3 stretching vibration of the butyl group.[6]

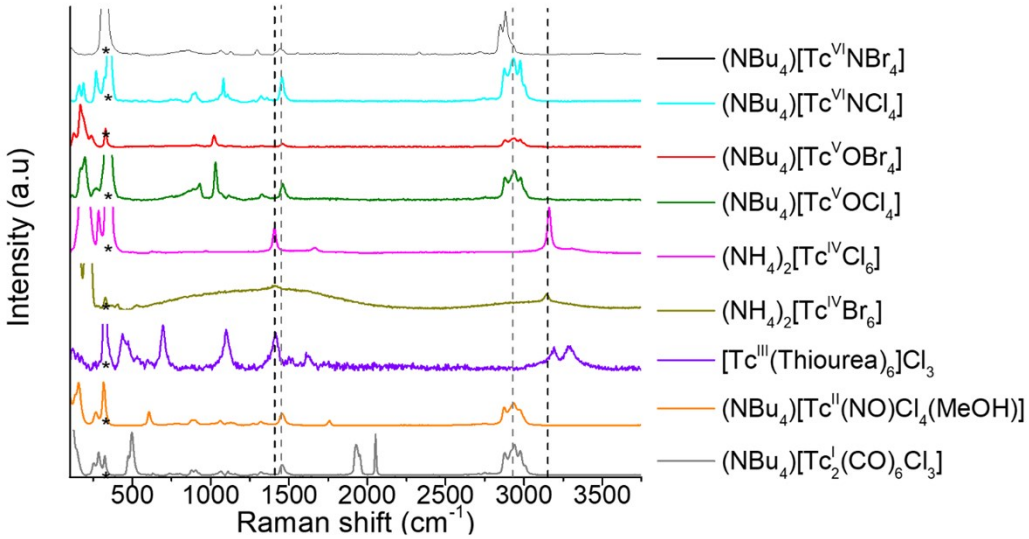

Figure S5. Raman spectra of various Tc compounds containing N-moieties as ligands or counter cations. Grey dashed lines correspond to the vibrations of NBu_4^+ and black dashed lines correspond to the vibrations of NH_4^+. The peak marked as (*) corresponds to CaF_2.

In addition to those bands, $(NBu_4)[Tc^{II}NOBr_4]$ and $(NBu_4)[Tc^{II}(NO)Cl_4(MeOH)]$ spectra have two bands at 614 and 1773 cm^{-1} and 607 and 1758 cm^{-1}, respectively. These values are in the range observed for NO vibrations when coordinated to different central atoms.[7]

In contrast, the spectrum of $[Tc^{III}(Thiourea)_6]Cl_3$ is different from the ones shown in the Figure S5. The spectrum possesses several peaks with high intensity: 473, 694, 1414, 1608, 3191 and 3296 cm^{-1}. These peaks are related to the C=S and NH_2 vibrations in thiourea.[8]

Tc K edge XANES

The Tc K edge XANES spectra were recorded at the Rossendorf Beamline (BM20) of the European Synchrotron Radiation Facility (ESRF), Grenoble, France.[9] This bending magnet beamline operates with Rh-coated mirrors for the collimation and reduction of higher harmonics. An energy range from 20.840 eV to 21.904 keV was scanned using Si(111) crystals with a varying step size down to 0.5 eV in the edge region. The samples were mounted between two ionization chambers for transmission detection XANES measurements.

Figure S6 shows the general complexity of interpreting Tc K-edge XANES data in a straightforward way. It is clear linking the white line energy, with any method available, with the oxidation state of the measured compounds serves no real purpose. Tc K-edge data is typically used in environmental science to determine the amount of Tc^{VII} present or in nuclear science by using linear combination fitting to distinguish Tc^{IV} and Tc^{VII}, the most commonly found oxidation states of Tc in the environment.[10,11] The Tc K-edge pre-edge peak originates mainly from a dipole forbidden 4d←1s transition due to p orbital mixing.[12] Similar to 3d transition metals like Fe, these interactions are more allowed when centrosymmetry is broken, for instance when the compound is not in an octahedral structure.[13]

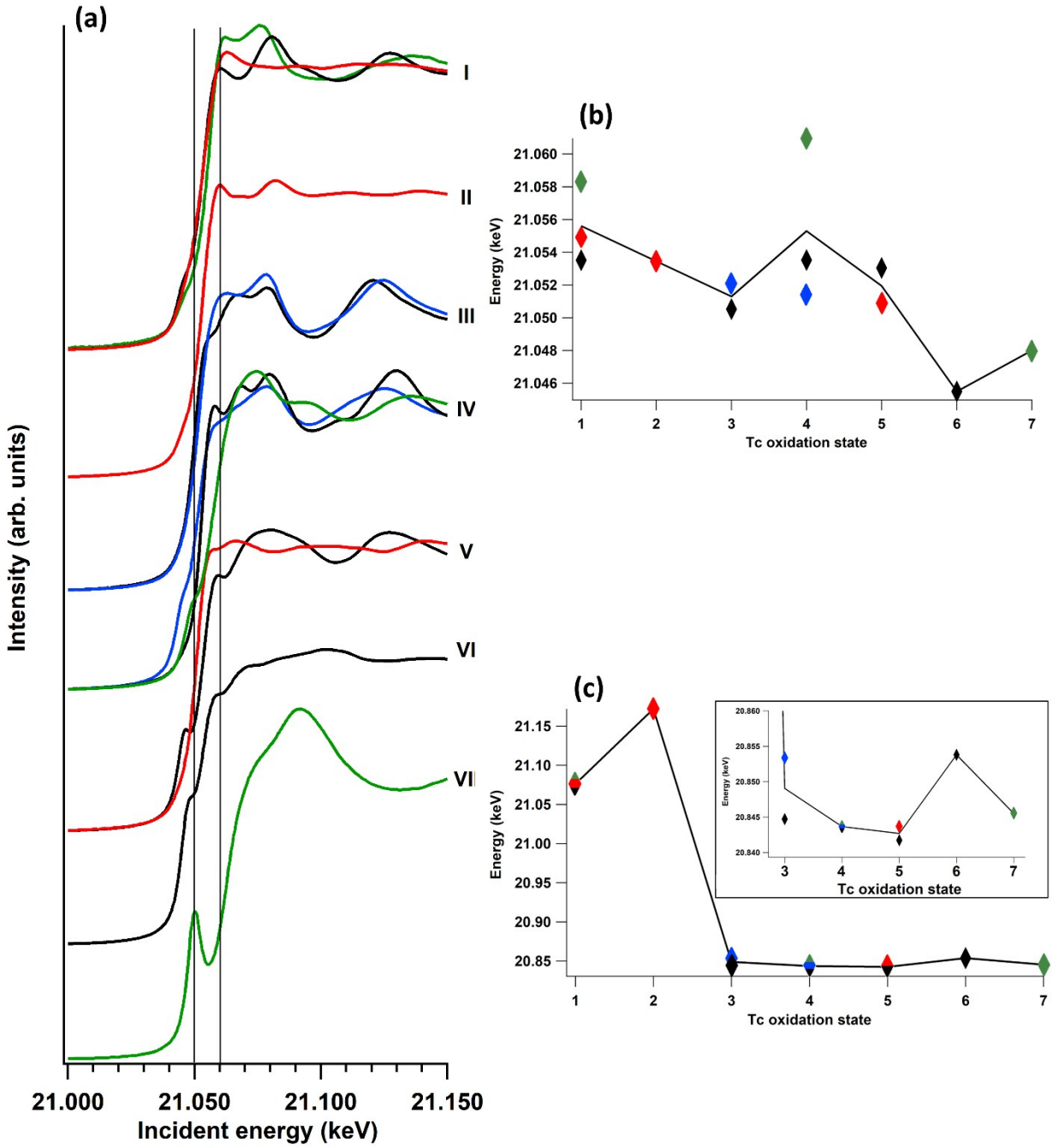

Figure S6. (a) Experimental Tc K edge XANES data for the Tc compounds. I includes $[Tc(NO)(NH_3)_4F](HF_2)$ *[green]*, $(NBu_4)[Tc_2(CO)_6Cl_3]$ *[black]* and $[Tc(NO)(Cp)Br(PPh_3)]$ *[red]*. II is $[Tc(NO)(Cp)Br(PPh_3)]Br$. III includes $[Tc(Thioharnstoff)_6]Cl_3$ *[black]* and $[TcCl_3(PPh_3)_2(CH_3CN)]$ *[blue]*. IV includes $[TcCl_4(PPh_3)_2]$ *[blue]* and $K_2[TcCl_6]$ *[black]*. V includes $(NBu4)[TcOCl_4]$ *[black]* and $(NBu_4)[TcOBr_4]$ *[red]*. VI is $(NBu_4)[TcNCl_4]$ and VII is $KTcO_4$. (b) shows the white line position based on the first inflection point and (c) based on the centre of mass method.

Syntheses and structures of the Tc compounds:

$(NBu_4)[Tc^{I}_2(\mu\text{-}Cl)_3(CO)_6]$

Synthesis: $(NBu_4)[BH_4]$ (1.25 g, 5.0 mmol) was dissolved in 3 mL of THF. CO gas was bubbled through the solution for 1 h. $(NBu_4)[TcOCl_4]$ (499 mg, 1.0 mmol) dissolved in 4 ml of THF was dropwise added over a period of 1 h with continuous CO gas supply. The resulting solution was stirred for 1 h at room temperature under a CO atmosphere and finally the solvent was removed by a stream of nitrogen. The resulting pale brown residue was dissolved in ethanol (6 mL) and 4 mL HCl (37%) was added. A colourless solid deposited after stirring the mixture at room-temperature overnight, which was filtered off, washed twice with water and i-propanol. Yield: 287 mg (80%). Elemental analysis: calcd for $C_{22}H_{36}Cl_3NO_6Tc_2$: Tc 27.7 %, found: Tc 27.6 %. The IR and NMR spectral data were identical with those published in ref. 14.

Structure:

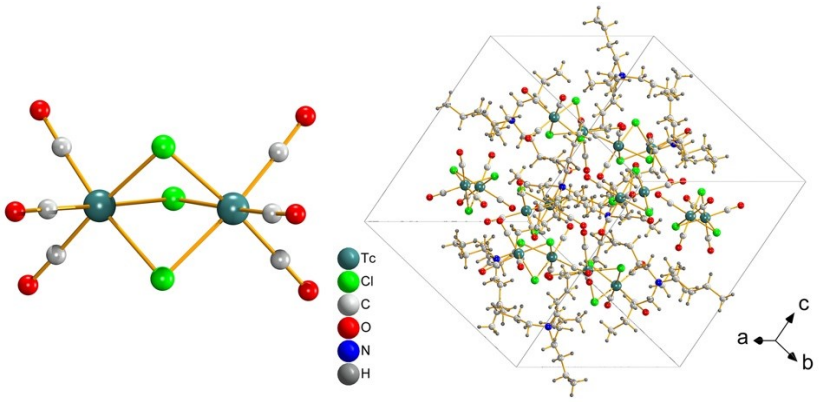

Figure S7. Molecular structure of the complex anion and unit cell packing of $(NBu_4)[Tc_2(\mu\text{-}Cl)_3CO)_6]$.[14]

$(NBu_4)[Tc^{II}(NO)Cl_4(MeOH)]$

Synthesis: The compound was prepared as described in ref. 15. Green crystals were obtained from slow evaporation of a CH_2Cl_2/MeOH mixture. Elemental analysis: calcd for $C_{19}H_{46}N_2O_3Cl_6Tc$ (for $(NBu_4)[Tc(NO)Cl_4(MeOH)]\cdot CH_2Cl_2\cdot MeOH$): Tc 14.9%; found: Tc 14.8%. IR and EPR spectral data were identical with those published in ref. 15.

Structure:

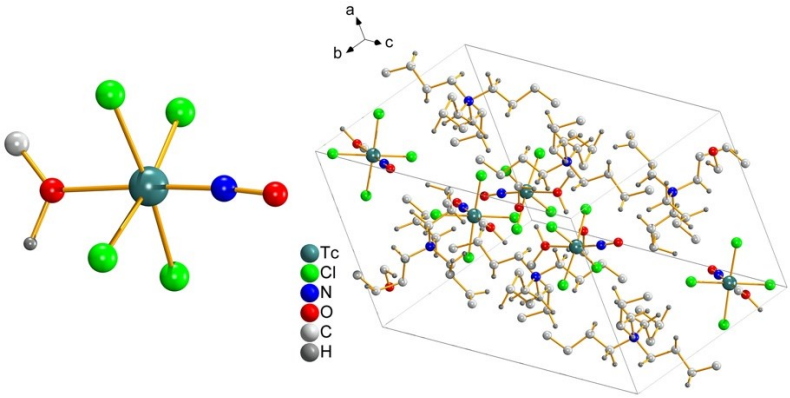

Figure S8. Molecular structure of the complex anion and unit cell packing of $(NBu_4)[Tc(NO)Cl_4(MeOH)] \cdot MeOH$.[16]

[$Tc^{III}Cl_3(PMe_2Ph)_3$]

Synthesis: The compound was prepared as described in ref. 17. Green crystals were obtained from slow evaporation of a MeOH mixture. Elemental analysis: calcd for $C_{24}H_{33}Cl_3P_3Tc$: Tc 16.0%; found: Tc 15.8%. IR data are identical with those published in ref. 17.

Structure:

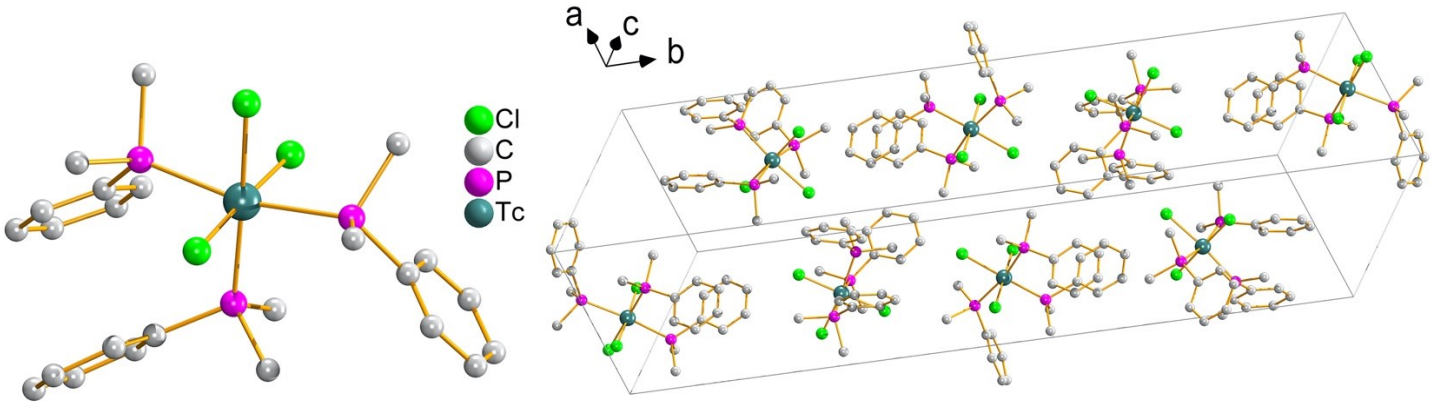

Figure S9. Molecular structure and unit cell packing of [$Tc^{III}Cl_3(PPhMe_2)_3$].[18]

[Tc^{III}(thiourea)$_6$]Cl_3

Synthesis: The compound was prepared as described in ref. 19. A red solid deposited directly from the reaction mixture. Elemental analysis: calcd for $C_6H_{24}Cl_3N_{12}S_6Tc$: Tc 14.9%; found: Tc 14.6%. IR data are identical with those published in ref. 19.

Structure:

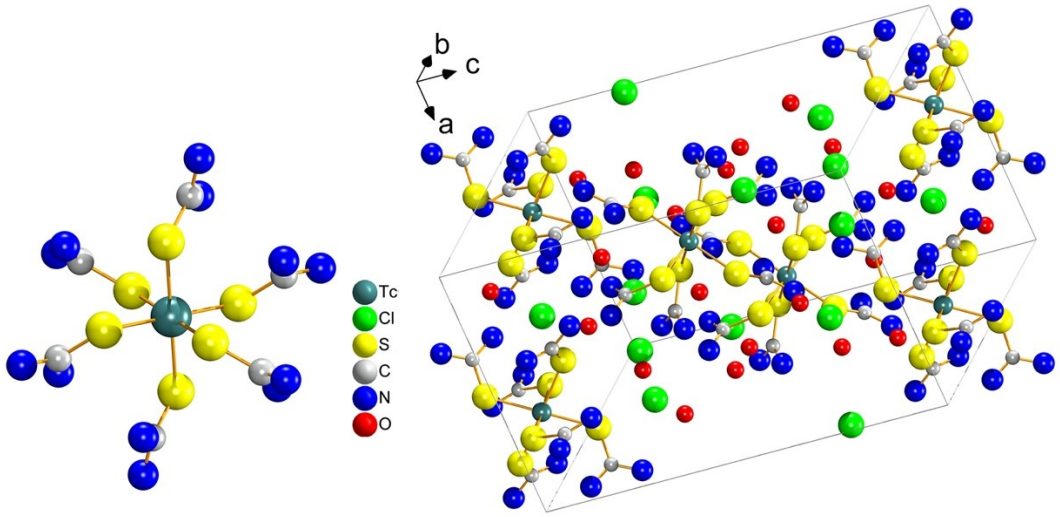

Figure S10. Structure of the complex cation and unit cell packing of [Tc^{III}(thiourea)$_6$]$Cl_3 \cdot 4\ H_2O$.[19]

[$Tc^{IV}Cl_4(PPh_3)_2$]

Synthesis: The compound was prepared from pertechnetate, PPh_3 and HCl as described in ref. 17. An almost insoluble green solid deposited directly from the reaction mixture. Elemental analysis: calcd for $C_{36}H_{30}Cl_4P_2Tc$: Tc 12.9%; found: Tc 12.9%. IR data are identical with those published in ref. 17.

Structure:

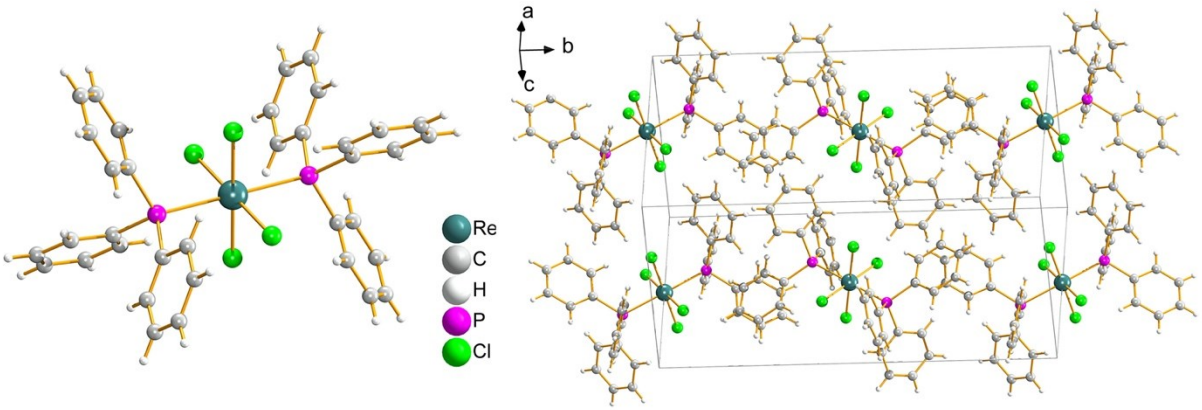

Figure S11. Molecular structure and unit cell packing of [$Re^{IV}Cl_4(PPh_3)_2$],[20] as equivalent for [$Tc^{IV}Cl_4(PPh_3)_2$].

$(NH_4)_2[Tc^{IV}Cl_6]$

Synthesis: $(NH_4)TcO_4$ (18 mg, 0.2 mmol) was dissolved in 5 mL of HCl (37%) and heated under reflux for 1 h. The colour of the solution changed to yellow. Some drops of aqueous NH_3 were added and the solution was concentrated to about 0.5 mL. Yellow crystals precipitated upon cooling. Yield: 61 mg (89%). Elemental analysis: calcd for $N_2H_8Cl_6Tc$: Tc 28.5%; found: Tc 28.5%.

Structure:

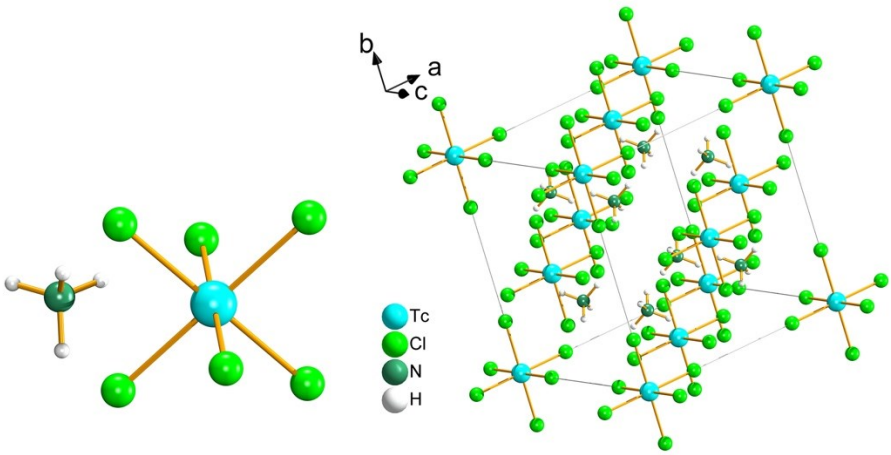

Figure S12. Ion structures and unit cell packing of $(NH_4)_2[Tc^{IV}Cl_6]$ (cubic, space group Fm-3m, a = b = c = 9.758(1) Å; M_w = 346.84 g/mol; yellow cubes, size 0.2·0.2·0.2 mm^3; density 2.479; measuring temperature 293(2) K; STOE IPDS 2T; radiation Mo Kα; theta range 3.616 – 26.962; index range h: -5 – 12, k: -9 – 12, l: -12 – 10; μ = 3.200 mm^{-1}; absorption correction XSHAPE: T_{max} = 0.7532, T_{min} = 0.5942; 71 reflections, 8 parameters, 1 restraint; R_{int} = 0.0477; wR_2 = 0.0954; R_1 = 0.03744; GOOF = 1.325. Deposition number CSD-1984500.

$(NH_4)_2[Tc^{IV}Br_6]$

Synthesis: $(NH_4)TcO_4$ (18 mg, 0.2 mmol) was dissolved in 5 mL of HBr (65%) and heated under reflux for 1 h. The colour of the solution changed to deep red. Some drops of aqueous NH_3 were added and the solution was concentrated to about 0.5 mL. Red-brown crystals precipitated upon cooling. Yield: 105 mg (85%). Elemental analysis: calcd for $N_2H_8Br_6Tc$: Tc 16.1%; found: Tc 16.3%.

Structure:

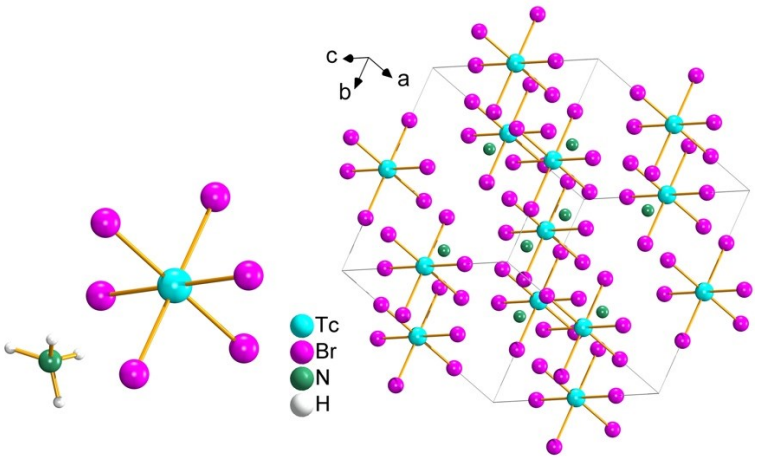

Figure S13. Ion structures and unit cell packing of $(NH_4)_2[Tc^{IV}Br_6]$ (cubic, space group Fm-3m, a = b = c = 10.398(2) Å; M_w = 613.54 g/mol; red-brown plate, size 0.3·0.25·0.07 mm³; density 3.625; measuring temperature 293(2) K; STOE IPDS 2T; radiation Mo Kα; theta range 3.919 – 26.963; index range h: -12 – 13, k: -13 – 13, l: -13 – 13; μ = 2.547 mm^{-1}; absorption correction XSHAPE: T_{max} = 0.6253, T_{min} = 0.2591; 89 reflections, 9 parameters; R_{int} = 0.1433; wR_2 = 0.0774; R_1 = 0361; GOOF = 1.255, Deposition number CSD-1984501.

$(NBu_4)[Tc^{V}OCl_4]$

Synthesis: The complex has been prepared according to the procedure of Preetz from $(NBu_4)TcO_4$ and HCl.[21] A gray-green solid is obtained. Elemental analysis: calcd for $C_{16}H_{36}NOCl_4Tc$: Tc 19.8%; found: Tc 20.2%. IR data were identical with those published in ref. 21.

Structure:

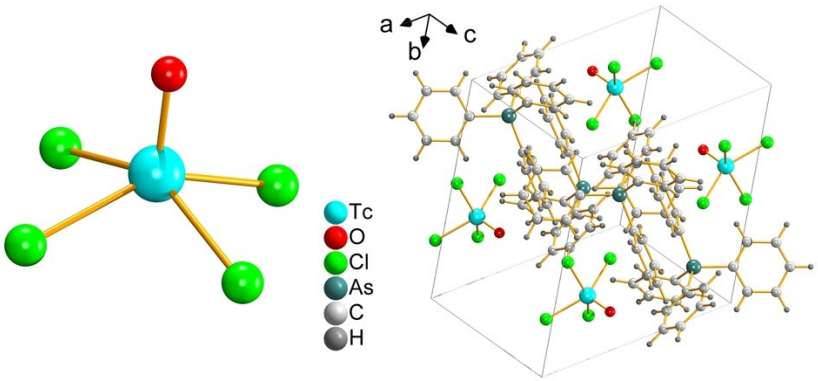

Figure S14. Structure of the complex anion and the unit cell packing of $(AsPh_4)[Tc^{V}OCl_4]$ as an equivalent structure for $(Bu_4N)[Tc^{V}OCl_4]$.[22]

$(NBu_4)[Tc^{V}OBr_4]$

Synthesis: The complex has been prepared according to the procedure of Preetz from $(NBu_4)TcO_4$ and HBr.[21] A gray-green solid is obtained. Elemental analysis: calcd for $C_{16}H_{36}NOBr_4Tc$: Tc 14.6%; found: Tc 14.3%. IR data were identical with those published in ref. 21.

Structure:

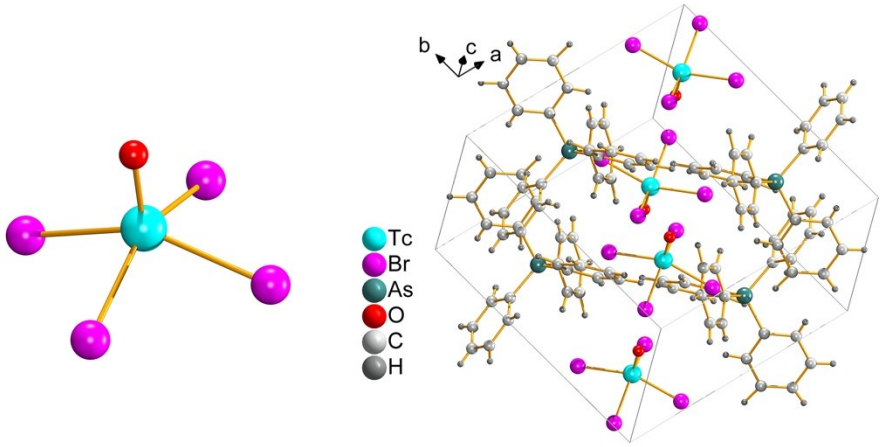

Figure S15. Structure of the complex anion and the unit cell packing of $(AsPh_4)[Tc^{V}OBr_4]$ as an equivalent structure for $(Bu_4N)[Tc^{V}OBr_4]$.[23]

$(NBu_4)[Tc^{VI}NCl_4]$

Synthesis: The complex has been prepared according to the procedure of Baldas et al.[24] Orange-red solid. Elemental analysis: calcd for $C_{16}H_{36}N_2Cl_4Tc$: Tc 19.9%; found: Tc 19.9%. IR data were identical with those published in ref. 24.

Structure:

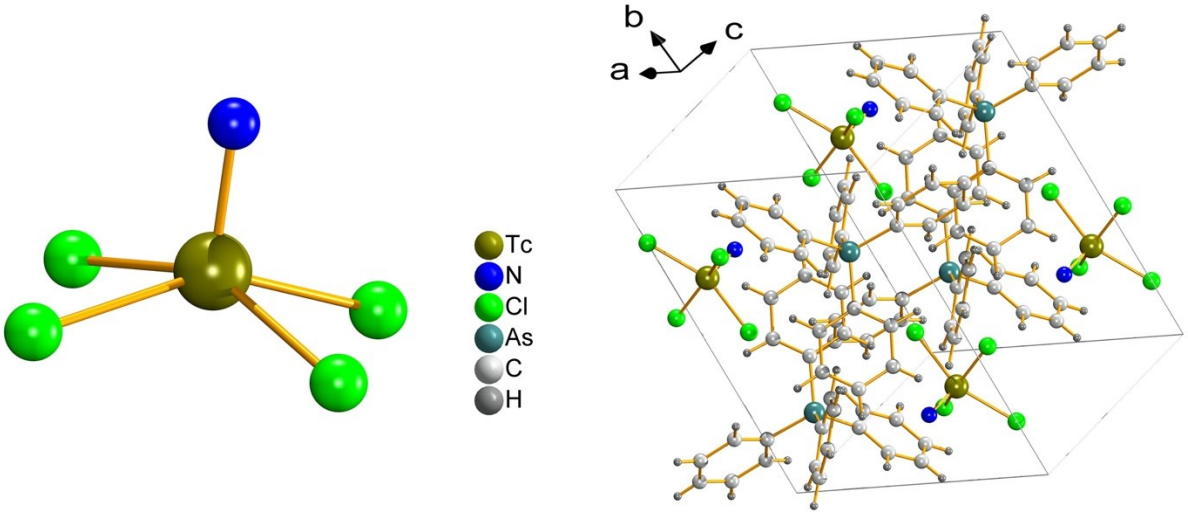

Figure S16. Structure of the complex anion and the unit cell packing of $(AsPh_4)[Tc^{VI}NCl_4]$ as an equivalent structure for $(Bu_4N)[Tc^{VI}NCl_4]$.[24]

$(NBu_4)[Tc^{VI}NBr_4]$

Synthesis: The complex has been prepared according to the procedure of Baldas et al.[24] Blue-purple solid. Elemental analysis: calcd for $C_{16}H_{36}N_2Br_4Tc$: Tc 14.7%; found: Tc 14.4%. IR data were identical with those published in ref. 24.

Structure:

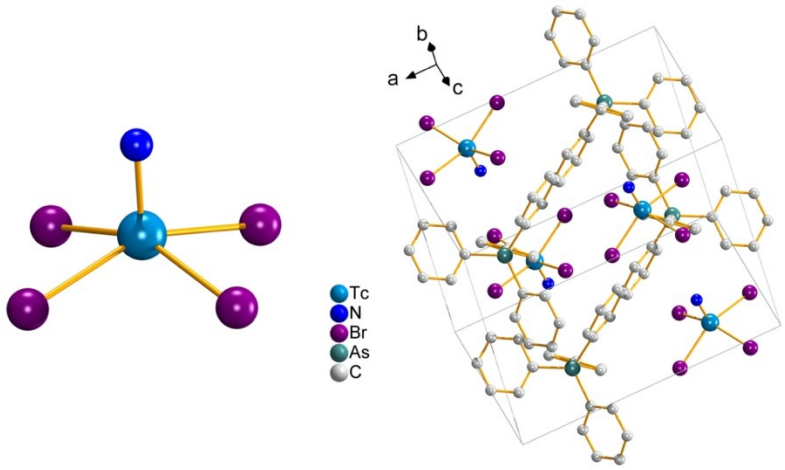

Figure S17. Structure of the complex anion and the unit cell packing of $(AsPh_4)[Tc^{VI}NBr_4]$ as an equivalent structure for $(Bu_4N)[Tc^{VI}NBr_4]$.[25]

$KTc^{VII}O_4$

Synthesis: The complex has been prepared from an aqueous solution of $(NH_4)TcO_4$ and KOH. Concentration of such solutions give colourless crystals of $KTcO_4$. Elemental analysis: calcd for O_4TcK: Tc 49.0%; found: Tc 49.1%. IR data were identical with those published in ref. 26.

Structure:

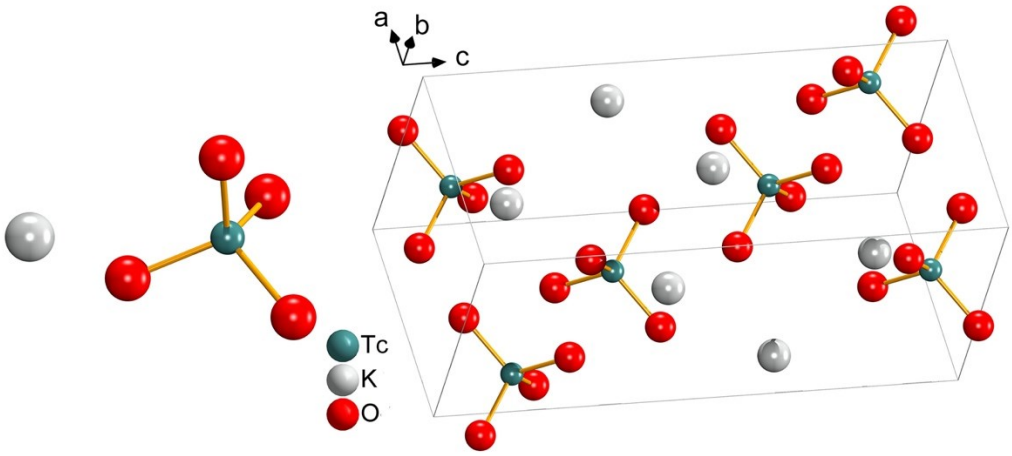

Figure S18. Structures of the ions and unit cell packing of $KTc^{VII}O_4$.[27]

Theoretical simulations in the framework of crystal-field multiplet theory

In general, the degree of the delocalization of d states increases for higher oxidation states, thus leading to stronger hybridization effects. In crystal-field multiplet theory, this is usually counteracted by a larger reduction of the values of the Slater integrals. Indeed, our calculations for higher oxidation states of Tc (Tc(V) – Tc(IV)) produced somewhat better results with a reduction of Slater integrals to values below 80% but not for all compounds. This can be connected to the fact that real local symmetries in those compounds were distorted from the approximated symmetries used in calculations.

The crystal-field parameters used in the calculations were adjusted to obtain the best agreement in spectral shape with the experiment. First, the 10Dq parameter was varied, then the Ds and Dt parameters to reproduce the specific spectral structures observed in recorded spectra.

The 1.6-eV Lorentzian broadening was chosen based on the core-hole lifetime data available for the L3 level of Mo and Ru in tables by Campbell et al.[28] The 0.5-eV Gaussian broadening corresponds to the energy resolution of the INE beamline where our measurements were conducted and is based on experimental determination.

Calculations of spectra using crystal-field multiplet theory do not show significant differences between $4d^5$ (Tc(II)) and $4d^55s^1$ (Tc(I)) configurations for the same local symmetry around the Tc sites because the influence of the 5s electron is negligible in this specific case. The differences in the spectral shape between Tc(I) and Tc(II) compounds can be attributed to some differences in the local symmetry as well as some differences in the strength of hybridization between Tc 4d states and ligand states which are not taken into account in calculations.

REFERENCES

1 M. Newville, Rev. Mineral. Geochemistry, 2014, 78, 33–74
2 R. M. Trevorah, C. T. Chantler and M. J. Schalken, IUCrJ, 2019, 6, 586–602.
3 H. G. M. Edwards, I. R. Lewis and P. H. Turner, Inorg. Chim. Acta, 1994, 216, 191–199.
4 D. Li, N. Zhai, S. Xu, M. Zhang, C. Sun and H. Li, Spectrochim. Acta Part A Mol. Biomol. Spectrosc., 2019, 206, 314–319.
5 K. Nakamoto, Infrared and Raman Spectra of Inorganic and Coordination Compounds: Part A: Theory and Applications in Inorganic Chemistry, JOHN WILEY & SONS LTD, 2009.
6 E. del Puerto, A. Cuesta, S. Sanchez-Cortes, J. V Garcia-Ramos and C. Domingo, Analyst, 2013, 138, 4670–4676.
7 A. B. McQuarters, J. W. Kampf, E. E. Alp, M. Hu, J. Zhao and N. Lehnert, Inorg. Chem., 2017, 56, 10513–10528.
8 R. G. Kumari, V. Ramakrishnan, M. L. Carolin, J. Kumar, A. Sarua and M. Kuball, Spectrochim. Acta Part A Mol. Biomol. Spectrosc., 2009, 73, 263–267.
9 W. Matz, N. Schell, G. Bernhard, F. Prokert, T. Reich, J. Claußner, W. Oehme, R. Schlenk, S. Dienel, H. Funke, F. Eichhorn, M. Betzl, D. Pröhl, U. Strauch, G. Hüttig, H. Krug, W. Neumann, V. Brendler, P. Reichel, M. A. Denecke and H. Nitsche, J. Synchrotron Radiat., 1999, 6, 1076–1085.
10 W. W. Lukens, D. A. McKeown, A. C. Buechele, I. S. Muller, D. K. Shuh and I. L. Pegg, Chem. Mater., 2007, 19, 559–566.
11 D. Li, J. C. Seaman, D. I. Kaplan, S. M. Heald and C. Sun, Chem. Eng. J., 2019, 360, 1–9.
12 K. Getty, M. U. Delgado-Jaime and P. Kennepohl, Inorganica Chim. Acta, 2008, 361, 1059–1065.
13 T. Yamamoto, X-Ray Spectrom., 2008, 37, 572–584.
14 R. Alberto, R. Schibli, D. Angst, P. A. Schubiger, U. Abram, S. Abram and T. A. Kaden, Transit. Met. Chem., 1997, 22, 597–601.
15 J. Ackermann, C. Nijki Noufele, A. Hagenbach and U. Abram, Z. Anorg. Allg. Chem. 2019, 645, 8-13.
16 D. S. Brown, J. L. Newman, J. R. Thornback and A. Davison, Acta Crystallogr. Sect. C Cryst. Struct. Commun.1987, 43, 1692–1694.
17 U. Mazzi, G. dePaoli, P.diBernardo and L. Magon, J. Inorg. Nucl. Med. 1976, 38, 721-725.
18 G. Bandoli, D. A. Clemente and U. Mazzi, Dalton Trans., 1976, 125.
19 M. J. Abrams, A. Davison, R. Faggiani, A. G. Jones and C. J. L. Lock, Inorg. Chem., 1984, 23, 3284–3288.
20 H. Kraudelt, U. Schilde and E. Uhlemann, Z. Anorg. Allg. Chem. 1995, 621, 1797–1799.
21 W. Preetz and G. Peters, Z. Naturforsch. B, 1980, 35, 1355-1358.
22 J. Baldas and S. F. Colmanet, Aust. J. Chem., 1989, 42, 1155–1159.
23 R. Hübener and U. Abram, Z. Anorg. Allg. Chem., 1992, 617, 96–98.
24 J. Baldas, J. F. Boas, J. Bonnyman and G. A. Williams, Dalton Trans., 1984, 2395.
25 J. Baldas, J. Bonnyman and G. A. Williams, Aust. J. Chem., 1985, 38, 215–219.
26 A. Müller and W. Rittner, Spectrochim. Acta A, 1967, 23, 1831-1837.
27 B. Krebs and K.-D. Hasse, Acta Crystallogr. Sect. B, 1976, 32, 1334–1337.
28 J. L. Campbell and T. Papp, At. Data Nucl. Data Tables, 2001, 77, 1–56.